Brown University
DIVISION OF ENGINEERING
PROVIDENCE, R.I. 02912

FRACTURE INITIATION DUE TO ASYMMETRIC IMPACT LOADING OF AN EDGE CRACKED PLATE

by

Y. J. Lee and L. B. Freund

(1)

FRACTURE INITIATION DUE TO ASYMMETRIC IMPACT LOADING OF AN EDGE CRACKED PLATE

by

Y. J. Lee and L. B. Freund

Office of Naval Research
Contract N00014-87-K-0481

National Science Foundation
Grant DMR-8714665

November 1988

FRACTURE INITIATION DUE TO ASYMMETRIC IMPACT LOADING OF AN EDGE CRACKED PLATE

Y. J. Lee
Research Assistant

and

L. B. Freund*
Professor of Engineering

Division of Engineering
Brown University
Providence, RI 02912

ABSTRACT

The two dimensional elastodynamic problem of a semi-infinite plate containing an edge crack is considered. Initially, the plate is stress free and at rest. To simulate the asymmetric impact of a projectile on the cracked edge of the plate, a normal velocity is suddenly imposed on the boundary of the plate on one side of the edge crack. The boundary of the plate and the crack faces are otherwise traction free. Due to the nature of the loading, a combined mode I and mode II transient stress intensity factor is induced at the crack tip. This stress intensity factor history is determined exactly by linear superposition of several more readily obtainable stress wave propagation solutions, including a fundamental solution arising from a particular problem in the dynamic theory of the elastic dislocations. The stress intensity factor histories are determined for the time interval from initial loading until the first scattered wave at the crack tip is reflected at the edge and arrives at the crack tip again. For an applied velocity with step function time dependence, the mode I stress intensity factor monotonically decreases and that of mode II increases until the arrival of the Rayleigh wave, it then slightly decreases for short duration, and then increases again. In experiments on fracture initiation in a high strength steel based on essentially this specimen and loading configuration, Kalthoff and Winkler (1987) reported that the fracture either grew off at an angle as a tensile crack or strain ahead as a shear fracture, depending on the intensity of the applied loading. The observations are considered in light of the solution reported here. (JES/AW)

* Fellow ASME

1. INTRODUCTION

An experimental technique has been proposed by Kalthoff and Winkler (1987) and Kalthoff (1987) for subjecting edge cracks in plate specimens to very high rates of loading that result in a crack tip deformation field that is predominantly mode II, that is, the in-plane shearing mode. A plate specimen with two parallel edge cracks or notches is impacted by a cylindrical projectile of diameter equal to the spacing between the cracks, as shown schematically in Fig. 1. Upon impact, the projectile produces a compressive wave in the part of the specimen between the two cracks, and this wave propagates toward the crack tips while merely grazing the two crack faces that border this part of the specimen. Upon arrival of the wave at the crack tips, the stiffness constraint of the remainder of the specimen is encountered and relatively large shear stress is induced on the crack planes ahead of the crack tips resulting in transient mode II stress intensity factors. The same idea has been applied by Kalthoff and co-workers for the case of a plate with a single edge crack.

The wave motion in the part of the specimen between the cracks upon projectile impact is actually much more complicated than the above discussion would suggest. A plane compressive wave is indeed generated upon impact. Because the crack faces are free of traction, cylindrical unloading waves immediately begin to propagate outward from the corners where the crack faces intersect the impacted edge of the plate. The wavefront diagram is shown in Fig. 2. These unloading waves have two main effects. They tend to erode the strength of the compressive plane wave as it propagates along the crack faces and they tend to result in outward bulging of the crack faces as the intense compression of the plane wave is relieved due to the presence of the free surface. These features are evident in some early work by Skalak (1957) on longitudinal wave propagation in a plate due to impact of the edge of the plate. The net result of the impact loading is to induce a transient, mixed-mode stress intensity factor field at the crack tip. The mode II stress intensity has a large component due to the main compressive wave, but a time dependent mode I stress intensity factor is also generated. In view of the tendency for the crack to close noted above, the mode I stress intensity factor will likely be negative.

Data are reported by Kalthoff (1987) for experiments on specimens of a high strength maraging steel. The plate dimensions were approximately $1\,cm \times 10\,cm \times 20\,cm$, and the crack

length, crack separation distance and projectile diameter were all about $5\,cm$. Impact velocities were in the range from about $10\,m/s$ to $100\,m/s$. A particularly interesting feature of the data is that two completely different failure modes were observed to occur, depending on the impacting speed of the projectile. For the lowest impact velocities, fracture occurred in the form of planar crack growth in a direction inclined at about 70° to the original crack plane. For impact speed greater than about $20\,m/s$, on the other hand, failure occurred by the crack-like growth of a shear band in a direction almost coincident with the original crack plane.

The purpose here is to compute the transient mixed mode stress intensity factors through analysis of a boundary value problem intended to model the experimental conditions in order to provide a broader basis on which to interpret the experimental results. The analysis here is based on the assumption of elastic material response, and study of the influence of crack tip plasticity is underway.

The particular edge cracked plate problem to be analyzed is shown schematically in Fig. 3. A rectangular x, y–coordinate system is introduced in the plane of the plate, and the plate occupies the half plane $x \geq -\ell$. A crack with traction free faces extends normally inward a distance ℓ from the edge of the plate. Thus, the crack tip is at the origin of coordinates as shown in Fig. 3. The normal stress component σ_{xx} vanishes on the edge of the plate for $y > 0$ and a time dependent normal velocity is imposed on the edge of the plate for $y < 0$. The shear traction is assumed to vanish everywhere on the plate edge.

To solve the problem, the longitudinal displacement potential ϕ and the shear displacement potential ψ are introduced through the Helmholtz decomposition of the displacement vector. The components of displacement in the coordinate directions are derived from the potentials by differentiation according to

$$u_x = \phi_{,x} + \psi_{,y} \qquad u_y = \phi_{,y} - \psi_{,x} \tag{1.1}$$

where the familiar comma-subscript notation is used to denote partial differentiation.

Each of these potential functions satisfies a two dimensional wave equation,

$$\phi_{,xx} + \phi_{,yy} - a^2\phi_{,tt} = 0 \qquad \psi_{,xx} + \psi_{,yy} - b^2\psi_{,tt} = 0 \tag{1.2}$$

where $a = 1/c_d = \sqrt{\rho/(\lambda+2\mu)}$ and $b = 1/c_s = \sqrt{\rho/\mu}$ are the inverse dilatational and shear waves speeds, respectively, in terms of the Lame elastic constants λ, μ and the mass density ρ. For future reference, $c = 1/c_R$ is the inverse Rayleigh wave speed.

The stress components can be expressed in terms of the displacement potentials by means of Hooke's law for the material. As already discussed above, the portion of the plate edge above the crack is completely traction free. On the other hand, the portion of the edge below the crack is free of shear traction, but the normal speed is imposed beginning at time $t = 0$. Thus, the solution must satisfy the boundary conditions

$$\begin{aligned} &\sigma_{xx}(-\ell, y, t) = 0, \qquad \sigma_{xy}(-\ell, y, t) = 0, \qquad && y > 0 \\ u_x(-\ell, y, t) = \int_0^t v(\tau)d\tau, \qquad &\sigma_{xy}(-\ell, y, t) = 0, \qquad && y < 0 \\ &\sigma_{xx}(x, 0^{\pm}, t) = 0, \qquad \sigma_{xy}(x, 0^{\pm}, t) = 0, \qquad && -\ell < x < 0 \end{aligned} \tag{1.3}$$

where $v(t)$ is prescribed for $t \geq 0$. The formulation is completed by specifying zero initial data. Evidently, the stress intensity factors will be identically zero until time $t = \ell/c_d$.

The boundary value problem formulated above is linear. Nonetheless, it is sufficiently complex so that known direct methods of solution are apparently not applicable. By studying the features of a sequence of sub-problems, however, it will be shown that mathematically exact expressions for the mode I and mode II stress intensity factors can be found. The property of linearity is exploited by superposition of these solutions in a certain way. The Laplace transform is useful in approaching some of these problems. The dual transform of the dilatational displacement potential $\phi(x, y, t)$ over time t and spatial coordinate x is defined by

$$\bar{\phi}(\xi, y, s) = \int_{-\infty}^{\infty} e^{-s\xi x} \int_0^{\infty} e^{-st}\, \phi(x, y, t)\, dt\, dx \tag{1.4}$$

where the transform parameters are defined to be s and $s\xi$, respectively. The parameter s may be viewed as a sufficiently large positive real number in considering transform on x.

The superposition scheme is outlined in Figs. 4, 5 and 6. In Fig. 4, it is shown that the asymmetric impact problem can be viewed as a superposition of a symmetric impact problem (A) and an antisymmetric impact problem (B). If $v(t)$ is the imposed normal velocity in the problem of interest, then a normal edge velocity of magnitude $\frac{1}{2}v(t)$ is imposed symmetrically

with respect to the crack plane in (A) and antisymmetrically with respect to the crack plane in (B). Thus, solutions of these two problems is required.

Consider the symmetric problem (A). It is shown in Fig. 5 that this problem can be decomposed into a quarter plane problem (C) and a problem concerned with the motion of dislocations emanating from the tip of a crack (D). The basic idea is as follows. If the imposed velocity begins to act on the edge $x = -\ell$ of the quarter plane in (C), then a normal displacement is induced on the edge $y = 0$. However, the displacement in the y–direction on $y = 0$ for the problem of interest (A) is zero. Consequently, the normal displacement induced on $x > 0$, $y = 0$ for the quarter plane problem (C) is canceled by a distribution of climbing edge dislocations emanating from the crack tip in (D) with a net displacement distribution on $y = 0$, $x > 0$ that exactly negates the normal displacement in (C). The use of dynamic dislocation solutions in this way was introduced by Freund (1974) in order to obtain stress intensity factor solutions for certain problems that are not amenable to direct analysis. These solutions have been used to interpret experimental data by Ravi-Chandar and Knauss (1984) and Kim (1985). A similar superposition scheme can be used to solve the antisymmetric loading problem.

Finally, the quarter plane problem can be solved by the superposition shown schematically in Fig. 6. Case (E) is the problem of a half plane occupying $x' = x + \ell \geq 0$ with the surface of the half plane subject to a uniform normal velocity $\frac{1}{2}v(t)$. A result of this loading is that a normal stress is induced on $y = 0$ for $x' < c_d t$. This normal stress is then negated by considering the problem (F) of a half plane occupying $y \geq 0$ subjected to a surface normal traction equal but opposite to that induced on $y = 0$ in (E). This approach was introduced by Wright (1969) and Freund and Phillips (1969) in studies of grazing incidence of a stress pulse on a free surface.

2. QUARTER PLANE PROBLEM

In this section, the solution of the quarter plane problem designated as (C) in the preceding discussion is determined. The plane strain deformation of an elastic material occupying the region $x' \geq 0$, $y \geq$ in the x, y–plane is considered, as indicated in Fig. 6. The prime on x is dropped for the development in this section. Initially, the material is stress free and at rest. At time $t = 0$, a spatially uniform normal displacement is imposed on the edge $x = 0$, $y > 0$ of the quarter plane. The shear traction is zero on this edge, and the traction is also zero on

the other edge $x > 0$, $y = 0$. The resulting wave motion is a plane wave at $x = c_d t$ that carries a unit jump in particle displacement in the x–direction, plus cylindrical dilatational and shear waves centered at the corner of the quarter plane with their associated headwaves. A Rayleigh wave is also expected on the free surface at $x = c_R t$.

For purposes of the superposition step indicated in Fig. 5 and its counterpart for the case of antisymmetric loading, the only feature of the solution of the quarter plane problem that is required is the displacement on the edge $y = 0$ for all time. It is this displacement that must be negated by a distribution of moving dislocations in (D). The displacement component $u_y(x,0,t)$ will lead to the mode I stress intensity factor, and likewise the component $u_x(x,0,t)$ will lead to the mode II stress intensity factor.

The two half plane problems whose superimposed solutions provide the solution for the quarter plane problem are labelled (E) and (F); see Fig. 6 for the case of symmetric loading. In (E), a unit step in normal displacement is imposed on the surface at time $t = 0$, and the shear traction on this surface is zero. The elementary solution is simply a plane wave propagating in the x–direction behind which $u_x = 1$. This wave satisfies the quarter plane boundary conditions on the edge $x = 0$, $y > 0$ but the boundary conditions on the other edge are violated. The plane wave induces no shear stress σ_{xy} on this surface but it does induce a compressive normal stress $-\lambda a \delta(t - x/c_d)$ where $\delta(\ )$ denotes the Dirac delta function. Thus, the solution of the half plane problem (F) must satisfy the boundary conditions

$$\sigma_{xy}(x,0,t) = 0, \qquad \sigma_{yy}(x,0,t) = \lambda a \delta(t - x/c_d)\,. \tag{2.1}$$

In considering the physical dimensions of terms in (2.1) and of other fields in this section, it should be kept in mind that all expressions are multiplied by a unit displacement.

Application of the Laplace transforms defined in (1.4) to the wave equations (1.2) and the boundary conditions (2.1) leads to the transformed wave potentials for problem (F) given by

$$\begin{aligned} \bar{\phi}^F(\xi,y,s) &= \frac{\lambda}{\mu}\frac{1}{s^2}\frac{a(b^2-2\xi^2)}{R(\xi)} g(\xi) e^{-s\alpha y} \qquad && \mathrm{Re}(\alpha) \geq 0 \\ \bar{\psi}^F(\xi,y,s) &= \frac{\lambda}{\mu}\frac{1}{s^2}\frac{2a\xi\alpha}{R(\xi)} g(\xi) e^{-s\beta y} \qquad && \mathrm{Re}(\beta) \geq 0 \end{aligned} \tag{2.2}$$

where $\alpha(\xi)$ and $\beta(\xi)$ are defined by

$$\alpha(\xi) = (a^2 - \xi^2)^{\frac{1}{2}}, \qquad \beta(\xi) = (b^2 - \xi^2)^{\frac{1}{2}} \tag{2.3}$$

and

$$\begin{aligned} g(\xi) &= \frac{1}{a-\xi} + \frac{1}{a+\xi} \\ R(\xi) &= (b^2 - 2\xi^2)^2 + 4\xi^2\alpha\beta\,. \end{aligned} \tag{2.4}$$

The superscript F indicates a feature of problem (F). The condition $\mathrm{Re}(\alpha) \geq 0$ is met for all points in the ξ–plane by cutting ξ–plane along $a \leq |\mathrm{Re}(\xi)| < \infty$, $\mathrm{Im}(\xi) = 0$, and choosing the branch for which α is a positive real number at $\xi = 0$. Similar conditions are imposed on β. The function $R(\xi)$ is recognized as the Rayleigh wave function, and the only roots of $R(\xi) = 0$ in the complex plane cut as indicated are at $\xi = \pm c = \pm 1/c_R$. The domain of definition of each of $\bar{\phi}$ and $\bar{\psi}$ is extended from the common strip of convergence of the integral transforms $-a < \mathrm{Re}(\xi) < a$ to the entire ξ–plane, cut along the line $|\mathrm{Re}(\xi)| > a$, $\mathrm{Im}(\xi) = 0$. Both $\bar{\phi}$ and $\bar{\psi}$ have simple poles at the zeros of $R(\xi)$. Furthermore, $\bar{\phi}$ has simple poles at $\xi = \pm a$, which correspond to the point loads on the surface of the half space propagating in opposite directions with the dilatational wave speed. Transformed displacements for (F) can be obtained from potentials in the form

$$\begin{aligned} \bar{u}_x^F(\xi,0,s) &= -\frac{\lambda}{\mu}\frac{1}{s}\frac{ab^2\xi(2\xi^2 - b^2 + 2\alpha\beta)g(\xi)}{R(\xi)} \\ \bar{u}_y^F(\xi,0,s) &= -\frac{\lambda}{\mu}\frac{1}{s}\frac{a\alpha(\xi)g(\xi)}{R(\xi)}\,. \end{aligned} \tag{2.5}$$

It is noted that the transformed form of u_x^F is similar to u_y of Lamb's (1904) problem and the transformed form of u_x^F is similar to u_y of Abou-Sayed *et al* , with a weighting function $g(\xi)$.

The displacement components in physical coordinates can be obtained by application of the Laplace transform inversion integrals and the Cauchy integral theorem. The displacement components for problem (C) are then obtained by superposition of the results from (E) and

(F), that is, $u_i^C = u_i^E + u_i^F$. The result is

$$u_x^C(x,0,t) = \begin{cases} \dfrac{\lambda}{\mu}\dfrac{a}{\pi}\displaystyle\int_a^{t/x} \mathrm{Im}\left(\frac{(b^2-2\xi^2)-2\alpha\beta}{R(\xi)}\right)\xi g(\xi)\,d\xi & ax < t < bx \\ \dfrac{\lambda}{\mu}\left[\dfrac{a}{\pi}\displaystyle\int_a^{b} \mathrm{Im}\left(\frac{(b^2-2\xi^2)-2\alpha\beta}{R(\xi)}\right)\xi a g(\xi)\,d\xi \right. & \\ \left. \quad + \dfrac{2c^2-b^2+2\sqrt{(c^2-a^2)(c^2-b^2)}}{2\kappa S(c)} g(c) H(t-cx)\right] & bx < t < \infty \end{cases} \tag{2.6}$$

and

$$u_y^C(x,0,t) = \frac{\lambda}{\mu}\frac{ab^2}{\pi}\int_a^{t/x} \mathrm{Im}\left(\frac{2a}{R(\xi)\sqrt{a^2-\xi^2}}\right) d\xi \qquad ax < t < \infty \tag{2.7}$$

where integration paths are taken on $\mathrm{Im}(\xi) \to 0^-$. The function $S(\xi)$ is defined in terms of the Rayleigh wave function by

$$R(\xi) = \kappa(c^2 - \xi^2)S(\xi) \tag{2.8}$$

where $\kappa = 2(b^2 - a^2)$. The function $S(\xi)$ has neither zeros nor poles in the cut ξ-plane and $S(\xi) \to 1$ as $|\xi| \to \infty$. With reference to Fig. 5, the displacement component u_y^C in (2.6) must be negated by superposition of dislocations in (D). The method to be described in the next section hinges on the observation that u_x^C and u_y^C are homogeneous functions of x and t of degree zero.

3. FUNDAMENTAL MOVING DISLOCATION SOLUTIONS

The next step in the analysis is to determine the crack tip stress intensity factor for a single edge dislocation climbing at constant speed out of the crack tip; see problem (D) in Fig. 5. The body is stress free and at rest up until the instant that the dislocation emerges from the crack tip. A solution to this problem that is valid for all time cannot be obtained in the presence of the free boundary at $x = -\ell$. However, a solution can be found for the case of a semi-infinite crack in an otherwise unbounded body, and the stress intensity factor histories will be identical cases for the two cases for time in the range $0 < t < 2\ell/c_d$. When the dislocation begins to move from the crack tip, a Rayleigh wave is initiated on the crack face. This surface wave travels at speed c_R from the crack tip toward the free edge of the plate. The main effect of free

surface in this case is to reflect the Rayleigh wave back toward the crack tip at time $t = \ell/c_R$. The reflected Rayleigh wave can have a significant effect on the stress intensity factor when it arrives back at the crack tip. It is expected that the difference in stress intensity factor histories for dislocation emission between the edge crack problem and the half plane crack problem will be small for time in the range $2\ell/c_d < t < 2\ell/c_R$.

Consider plane strain deformation of an unbounded elastic solid containing a half plane crack whose faces are free of traction. The material is initially stress free and at rest. At time $t = 0$, an elastic dislocation with Burgers vector of magnitude 2Δ in the y-direction begins to move at constant speed v in the positive x-direction from the crack tip. In the terminology of elastic dislocation theory, this is an edge dislocation climbing in the x-direction. The speed is assumed to be in the range $0 \leq v \leq c_d$, though the solution may be obtained by the same procedure if the speed exceeds the dilatational wave speed of the material.

For the case of mode I, the deformation is symmetric with respect to the plane $y = 0$. Thus a solution is sought for $-\infty < x < \infty, 0 < y < \infty$, and $0 \leq t < \infty$ subject to the boundary conditions

$$\begin{aligned} \sigma_{yy}(x,0,t) &= \sigma_+(x,t) \\ \sigma_{xy}(x,0,t) &= 0 \\ u_y(x,0,t) &= u_-(x,t) + \Delta H(vt - x) \end{aligned} \tag{3.1}$$

where σ_+ is the unknown normal stress distribution on the plane $y = 0$ for $x \geq 0$, and $\sigma_+ = 0$ for $x < 0$. Likewise u_- is the unknown normal displacement distribution on $y = 0$ for $x < 0$, and $u_- = 0$ for $x > 0$.

Following the procedure introduced by Freund (1974), the Wiener-Hopf equation for this case is

$$\frac{-b^2\alpha(\xi)}{\mu R(\xi)}\Sigma_+(\xi) = U_-(\xi) + \frac{\Delta}{\xi + d} \tag{3.2}$$

where Σ_+ and U_- are the double Laplace transforms of σ_+ and u_-, respectively, and $d = 1/v$. Application of the factorization procedure of the Wiener-Hopf method leads to the solution for the double transform of σ_+ in the form

$$\Sigma_+(\xi) = -\frac{\Delta\mu\kappa}{b^2}\frac{1}{(\xi + d)F_+(\xi)F_+(d)} \tag{3.3}$$

where

$$F_+(\xi) = \frac{(c+\xi)S_+(\xi)}{\alpha_+(\xi)} \tag{3.4}$$

and

$$S_\pm(\xi) = \exp\left\{-\frac{1}{\pi}\int_a^b \tan^{-1}\left[\frac{4\eta^2|\alpha||\beta|}{(2\eta^2-b^2)^2}\right]\frac{d\eta}{\eta\pm\xi}\right\}. \tag{3.5}$$

The transform inversion leads to the expression for σ_+ in the physical domain as

$$\sigma_+(x,t) = -\frac{\Delta}{\pi x}\mathrm{Im}\left\{\Sigma_+(-\frac{t}{x}+i0)\right\}H(t-ax). \tag{3.6}$$

The stress intensity factor history for mode I due to the dislocation moving at speed v, say $k_I(t;v)$, may be deduced from the asymptotic behavior of $\Sigma_+(\xi)$ as $\xi\to\infty$, with the result

$$k_I(t;v) = -\sqrt{\frac{2}{\pi}}\frac{\mu\kappa}{b^2}\frac{1}{F_+(d)\sqrt{t}} \qquad (\Delta=1). \tag{3.7}$$

The fact that $\sigma_+(x,t)$ is a homogeneous function of its arguments of order -1 is evident in (3.6). Furthermore, the dependence of the stress intensity factor on the dislocation velocity v has been indicated explicitly in (3.7). These observations are important in calculating the transient stress intensity factor $K_I(t)$ for the crack problem (A). Recall that this step requires the superposition of dislocations that reproduces a normal displacement that is exactly equal but opposite to the normal displacement $u_y(x,0,t)$ of the quarter-plane problem (C); see Fig. 5.

The case of mode II can be handled in an analogous way. The direction of Burgers vector is the negative x-direction, rather than the positive y-direction as in mode I. In addition, the normal stress σ_{yy} vanished on $y=0$ in the mode II equivalent of problem (D) instead of the component σ_{xy} in mode I. Suppose that $\tau_+(x,t)$ is the unknown shear stress on $y=0$, $x>0$ in this case. Without repeating the details, it can be shown that

$$\tau_+(x,t) = \frac{1}{\pi x}\frac{\Delta\mu\kappa}{b^2}\mathrm{Im}\left\{\frac{1}{(\xi+d)G_+(\xi)G_+(d)}\right\}_{\xi=-t/x+i0}H(t-ax) \tag{3.8}$$

where

$$G_+(\xi) = \frac{(c+\xi)S_+(\xi)}{\beta_+(\xi)}. \tag{3.9}$$

The fundamental stress intensity factor solution is

$$k_{II}(t;v) = -\sqrt{\frac{2}{\pi}}\frac{\mu\kappa}{b^2}\frac{1}{G_+(d)\sqrt{t}} \qquad (\Delta=1). \tag{3.10}$$

The fundamental stress intensity factor solutions (3.7) and (3.10) will be used in the next section to construct the full mode I and mode II stress intensity factor histories.

4. MIXED MODE STRESS INTENSITY FACTORS

In the preceding section, the stress intensity factor due to the motion of a dislocation away from the tip of the crack at constant speed was considered. Suppose now that a continuous distribution of dislocations is emitted from the crack tip, each moving with a different constant speed. Furthermore, suppose that the time of emission and the amplitude of the Burgers displacement both depend on the speed of the dislocation. For any continuous variation of the amplitude, say $w(v)$, and the time of emission, say $t_o(v)$, with speed v the continuous distribution represents a displacement distribution that is a homogeneous function of degree zero of position and time. From (3.7) or (3.10), the stress intensity factor resulting from this dislocation distribution is

$$K(t) = -\int_{v_1}^{v_2} k(t - t_o; v)\,\frac{dw(v)}{dv}\,dv \tag{4.1}$$

where v_1 and v_2 are appropriate limits on the actual range of speed.

In the present case, the distribution of climbing edge dislocations giving rise to an opening displacement across the plane $y = 0$ results in the mode I stress intensity factor. Thus, w in (4.1) is replaced by u_y^C from (2.7). If the boundary loading acts at time $t = 0$ and at place $x = -\ell$, then the time at which the displacement level with speed x/t arrives at $x = 0$ is $t_o(v) = (1 - v/c_d)\ell/v$. The first displacement level to arrive at $x = 0$ does so with speed c_d, and the range of speeds of all displacement levels involved at time t is $\ell/t < v < c_d$. Therefore, the mode I stress intensity factor resulting from negation of the displacement distribution u_y^C, and the corresponding mode II stress intensity factor resulting from negation of u_x^C, are

$$K_I(t) = -\int_a^{h^*} k_I(t - t_o; h)\,\frac{du_y(h)}{dh}\,dh \tag{4.2}$$

$$K_{II}(t) = -\int_a^{h^*} k_{II}(t - t_o; h)\,\frac{du_x(h)}{dh}\,dh \tag{4.3}$$

where $h^* = t/\ell$ and the inverse speed $h = 1/v$ has been used as the integration variable for convenience. The integral expression for K_I can be evaluated by using the fundamental

formula for $k_I(t;v)$ in (3.7) and the explicit expression for the displacement u_y^C given in (2.7). The procedure is described by Freund (1974), and only the result is included here, that is,

$$K_I(t) = -\frac{\lambda}{\sqrt{2\pi\ell}} \begin{cases} \frac{\kappa}{\pi}\int_a^{h^*} \frac{2a^2(2h^2-b^2)P(h)}{(h+a)\sqrt{(h-a)(h^*-h)}}\,dh & a < h^* < b \\ \frac{\sqrt{2a}}{\sqrt{h^*+a}S_+(a)}\frac{a}{c+a} + \frac{2a^2\sqrt{c-a}}{\sqrt{c-h^*}S_-(c)(c^2-a^2)} & b < h^* < c \\ \frac{\sqrt{2a}}{\sqrt{h^*+a}S_+(a)\frac{a}{(c+a)}} & c < h^* < 3a \end{cases} \tag{4.4}$$

The history of K_I is square root singular at $t/\ell = c$, but a nonzero, finite value is obtained at $t/\ell = a$ from the integration. Following a similar process, K_{II} is obtained as

$$K_{II}(t) = -\frac{\lambda}{\sqrt{2\pi\ell}} \begin{cases} \frac{\kappa}{\pi}\int_a^{h^*} \frac{4a^2hP(h)\sqrt{b-h}}{\sqrt{(h^2-a^2)(h^*-h)}}\,dh & a < h^* < b \\ \frac{\kappa}{\pi}\int_a^{b} \frac{4a^2hP(h)\sqrt{b-h}}{\sqrt{(h^2-a^2)(h^*-h)}}\,dh & b < h^* < c \\ \frac{\kappa}{\pi}\int_a^{b} \frac{4a^2hP(h)\sqrt{b-h}}{\sqrt{(h^2-a^2)(h^*-h)}}\,dh & \\ \quad + \frac{2a^2c}{b^2(c^2-a^2)}\frac{2c^2-b^2-2\sqrt{(c^2-a^2)(c^2-b^2)}}{\beta_+(c)S_-(c)}\frac{1}{\sqrt{h^*-c}} & c < h^* < 3a \end{cases} \tag{4.5}$$

The history of K_{II} has a square root singularity at $t/\ell = c$, but again a finite value is found at $t/\ell = a$ from the integration. In the above expressions, $P(h) = (c+h)(2h^2-b^2)S_+(h)/[(2h^2-b^2)^4 + 16h^4(h^2-a^2)(b^2-h^2)]$.

For numerical evaluation of these expressions Poisson's ratio ν is assumed to be equal to 0.25. In this case, the ratios of the slowness are $b^2 = 3a^2$ and $c^2 = 3.549\,a^2$. The stress intensity factors have been evaluated numerically by application of the appropriate Gaussian quadrature rules with Chebychev polynomial interpolations. The results are shown in Fig. 7 and Fig. 8. The results are normalized by a factor that is the static mode II stress intensity factor as $t \to \infty$ for the problem posed in section 1 and shown schematically in Fig. 3. This stress intensity factor is easily calculated to be $E/[2(1-\nu^2)\sqrt{\pi\ell}]$ (times the unit imposed displacement) by means of the M-integral procedure introduced by Freund (1978).

Up to this point, the stress pulse grazing the lower edge of the crack surface has had the form of a displacement with step function time dependence. The stress intensity factors for

general time dependence can be obtained by convolution. If the velocity on the lower edge is prescribed as an arbitrary function of time $v(t)$, then the stress intensity factor for this situation is

$$\mathcal{K}(t) = \int_0^t K(t-s)v(s)\,ds\,. \tag{4.6}$$

For special example, suppose that the velocity is a step function $v(t) = v_o H(t)$, which is essentially the loading condition used by Kalthoff (1987). The resultant values of $\mathcal{K}_I(t)$ and $\mathcal{K}_{II}(t)$ obtained according to (4.6) are presented in Fig. 9 and Fig. 10. The normalizing factor here is $Ev_o\sqrt{\ell/\pi}\,/[2c_d(1-\nu^2)]$.

5. DISCUSSION

In the foregoing sections, the exact elastodynamic stress intensity factor history has been determined for a particular case of asymmetric impact of an edge cracked plate. The stress intensity factor results for impulsive imposed velocity $v(t) = \delta(t)$ are presented in Figs. 7 and 8. In themselves, these results are of limited practical significance. However, they provide the fundamental building block for determining the transient stress intensity factors for more realistic imposed velocity boundary conditions. In addition, the existence of an exact solution for a configuration of this sort provides a valuable check on numerical procedures that are being developed to analyze more complex geometries and, eventually, impact with nonlinear material response.

The exact stress intensity factor histories for step velocity loading $v(t) = v_o\,H(t)$ are given in Figs. 9 and 10. As anticipated, when the imposed velocity on the boundary is in a direction into the material, then the adjacent crack face bulges outward and the resulting mode I stress intensity factor is negative. If the crack is initially closed the faces would press against each other and, in fact, no mode I stress intensity factor would develop. On the other hand, if the crack is initially held open by some background equilibrium load or if the geometry is such that a small opening exists then the crack will indeed tend to close upon application of the boundary velocity.

The magnitude of the mode I stress intensity factor is always less than the magnitude of the corresponding mode II stress intensity factor, but the value is significant. A single parameter that is useful in characterizing the near tip field under mixed mode conditions was introduced

by Shih (1974). The parameter is defined by

$$\mathcal{M}^e = \frac{2}{\pi} \tan^{-1}\left(\frac{K_I}{K_{II}}\right) \tag{5.1}$$

and it is called the mixity parameter. The dependence of the mixity parameter on time for the problem analyzed here is shown in Fig. 11 where it is seen that the value varies only a small amount from 0.25 over the time interval of interest.

If it is assumed that the crack will grow in a direction determined by the condition that the circumferential tensile stress within the asymptotic field is maximum then the angle between the crack line and the direction of growth satisfies

$$3\sin^2(\frac{\theta}{2}) - \tan(\frac{\pi}{2}\mathcal{M}^e)\cos(\frac{\theta}{2})\sin(\frac{\theta}{2}) - 1 = 0\,. \tag{5.2}$$

The angle θ_e that satisfies this condition for the problem analyzed here is also shown in Fig. 11 where it is seen that this angle varies only slightly from 63° in the time interval of interest.

The possible influence of crack face interaction resulting from the tendency for the crack to close under compressive loading is difficult to assess at this point. In the pure mode I problem considered by Freund (1974) the crack could be view as closed with normal pressure acting or open with no traction acting. In the mixed mode case considered here, however, the crack faces would tend to slide with respect to each other if they are in contact so that the two modes are coupled in a way that has not yet been sorted out. Perhaps some progress on this point could be made by considering the case of closed crack faces, that is, continuous normal traction and velocity across the crack, but zero shear traction over the entire crack surface. This problem could be analyzed by the procedure used here.

Data taken from the work of Kalthoff (1987) is also shown in Fig. 10. He measured the speed of the impacting projectile in the configuration of Fig. 1, and the resulting stress intensity factor histories were observed by means of the optical shadow spot method. In his experiments, interaction between the crack faces was avoided by cutting the cracks into the plate so that there was a finite gap between the crack faces. Thus, both a mode II stress intensity factor and a *compressive* mode I stress intensity factor could be generated, as modeled in the present analysis. To enter this data for steel specimens struck by steel projectiles on Fig. 10, the velocity

value v_o imposed on the edge of the specimen was determined by assuming that the portion of the specimen struck by the projectile (see Fig. 1) had the same elastic impedance as the projectile itself. Thus, from elementary wave propagation theory, the value of v_o was essentially one-half of the speed of the incident projectile. The agreement between the analytical model results and the experimental results for the low velocity result ($v_o = 6.5\,m/s$) is excellent over the time range for which data are reported. On the other hand, the observed mode II stress intensity factor for the higher velocity impact ($v_o = 16.5\,m/s$) is less than the theoretical result up until the time $c_d t/\ell \sim 2$, and substantially above thereafter. Kalthoff (1987) also reported results of one experiment on the brittle plastic Araldite B which, when normalized, were closer to the analytical results than the high impact velocity steel results but which differed in the same general way. Nonetheless the trend between the observed variation of K_{II} with time and the analytical result are consistent in both cases up until $c_d t/\ell \sim 2$. The differences thereafter could be due to nonlinear material response in the crack tip region or to the influence of other features of the experiment not taken into account in the analytical model, such as the presence of the second crack. Both of these possibilities are being pursued through further work based on detailed numerical simulation of the process.

Some understanding of the role of crack tip processes in the interpretation of dynamic fracture data obtained by means of the optical shadow spot method has been achieved. The shadow spot image on a screen or camera is created as a locus of points of multiple mapping of a family of light rays influence by deformation of the specimen. The curve on the specimen that is geometrically mapped into the boundary of the shadow spot must be within a region where the mechanical fields are adequately represented by the asymptotic elastic crack tip field, and this condition imposes quite severe constraints on the method. The presence of a crack tip plastic zone can distort the shadow spot and increase its size so that the inferred value of stress intensity factor is not accurate (Rosakis and Freund, 1981). In the experiments reported by Kalthoff (1987) a well-defined shear band grew from the crack tip in the plane of the crack for the case of high velocity impact, and it is possible that the presence of the band influenced the inferred stress intensity factor values.

ACKNOWLEDGEMENT

The work described here was supported by the National Science Foundation, through grant DMR87-14665 to Brown University, and by the Office of Naval Research, through contract N00014-87-K-0481 to Brown University. This research support is gratefully acknowledged.

REFERENCES

[1] Abou-Sayed, I. S., Burgers, P., and Freund, L. B., 1980, "Stress Intensity Factor Due to Parallel Impact Loading of the Faces of a Crack," *Fracture Mechanics; Twelfth Conference, ASTM STP* 700, pp. 164–173.

[2] Freund, L. B., 1974, "The Stress Intensity Factor Due to Normal Impact Loading of the Faces of a Crack," *International Journal of Engineering Science*, Vol. 12, pp. 179–189.

[3] Freund, L. B., and Phillips, J. W., 1969, "Stress Pulse Grazing a Free Boundary of an Elastic Solid," *Brown University Technical Report*, No. A.M. 39.

[4] Freund, L. B., 1978, "Stress Intensity Factor Calculations Based on a Conservation Integral," *International Journal of Solids and Structures*, Vol. 14, pp. 241–250.

[5] Kalthoff, J. K., and Winkler, S., 1987, "Failure Mode Transition at High Rates of Shear Loading," *International Conference on Impact Loading and Dynamic Behavior of Materials.*

[6] Kalthoff, J. K., 1987, "Shadow Optical Analysis of Dynamic Shear Fracture," *International Conference on Photomechanics and Speckel Metrology*, SPIE, Vol. 814, pp 531–538.

[7] Kim, K. S., 1985, "Dynamic Fracture under Normal Impact Loading of the Crack Faces," *ASME Journal of Applied Mechanics*, Vol. 52, pp. 585–592

[8] Lamb, H., 1904, "On the Propagation of Tremors over the Surface of an Elastic Solid," *Philosophical Transactions of the Royal Society*, London, Series A, Vol. 203, pp. 1–42.

[9] Ravi-Chandar, K., and Knauss, W. G., 1984, "An Experimental Observation into Dynamic Fracture," in four parts, *International Journal of Fracture*, Part I: 25, pp. 247–262, Part II: 26, pp. 65–80, Part III: 26, pp. 141–154, Part IV: 26, pp. 189–200.

[10] Rosakis, A. J., and Freund, L. B., 1981, "The Effect of Crack-Tip Plasticity on the Determination of Dynamic Stress-Intensity Factors by the Optical Method of Caustics," *ASME Journal of Applied Mechanics*, Vol. 48, pp. 302–308.

[11] Shih, C. F., 1974, "Small-Scale Yielding Analysis of Mixed Mode Plane-Stain Crack Problems," *Fracture Analysis ASTM STP 560*, pp. 187–210.

[12] Skalak, R., 1957, "Longitudinal Impact of a Semi-infinite Circular Elastic Bar," *ASME Journal of Applied Mechanics*, Vol. 24, pp. 59–64.

[13] Wright, T. W., 1969, "Impact on an Elastic Quarter Space," *the Journal of the Acoustical Society of America*, Vol. 45, pp. 935–943.

FIGURE CAPTIONS

Figure 1. — Experimental configuration introduced by Kalthoff and Winkler (1987) for dynamic fracture initiation studies under mixed mode conditions.

Figure 2. — Pattern of wave fronts generated in the portion of the specimen shown in Fig. 1 between the two cracks due to normal impact of the projectile.

Figure 3. — A schematic representation of the boundary value problem considered here, showing the edge crack of length ℓ and the imposed normal velocity imposed asymmetrically on the edge of the plate.

Figure 4. — Decomposition of the asymmetric boundary value problem in Fig. 1 into a symmetric loading system (A) and an anti-symmetric loading system (B).

Figure 5. — Decomposition of problem (A) into a quarter plane problem (C) and a dynamic dislocation propagation problem (D).

Figure 6. — Decomposition of the quarter plane problem (C) into two half plane problems, each of which can be solved by standard methods of analysis.

Figure 7. — The mode I stress intensity factor for the case of impulsive imposed velocity $v(t) = \delta(t)$, normalized by $E/[2(1-\nu^2)\sqrt{\pi\ell}]$, versus normalized time.

Figure 8. — The mode II stress intensity factor corresponding to the result in Fig. 7.

Figure 9. — The mode I stress intensity factor for the case of step loading $v(t) = v_o\, H(t)$, normalized by $Ev_o\sqrt{\ell/\pi}/[2(1-\nu^2)c_d]$, versus normalized time.

Figure 10. — The mode II stress intensity factor corresponding to the result in Fig. 9. The data points are those reported by Kalthoff (1987).

Figure 11. — The mixity parameter defined in (5.1) for the stress intensity factors given in Figs. 9 and 10, and the corresponding direction of crack growth based on a maximum circumferential tensile stress criterion.

I By

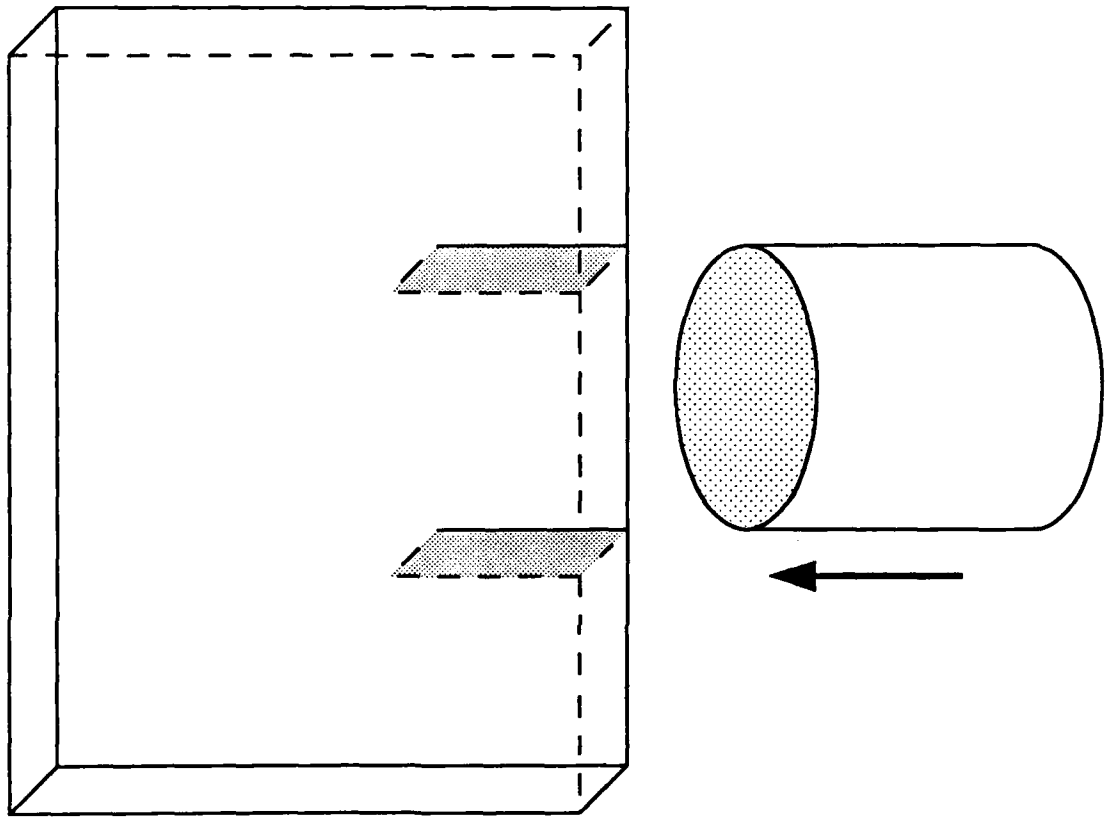

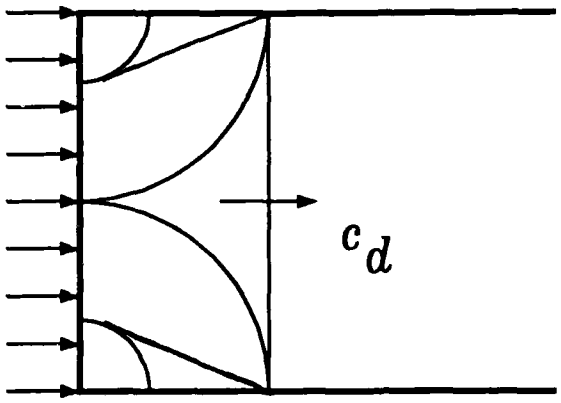

Fig 2

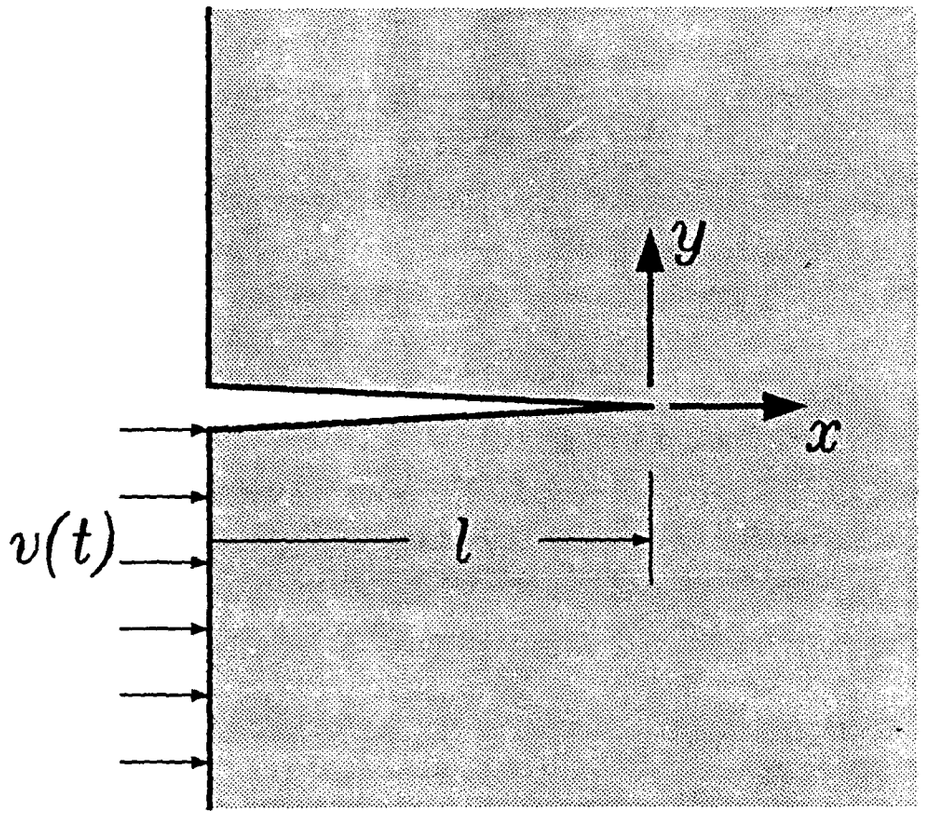

Fig 3

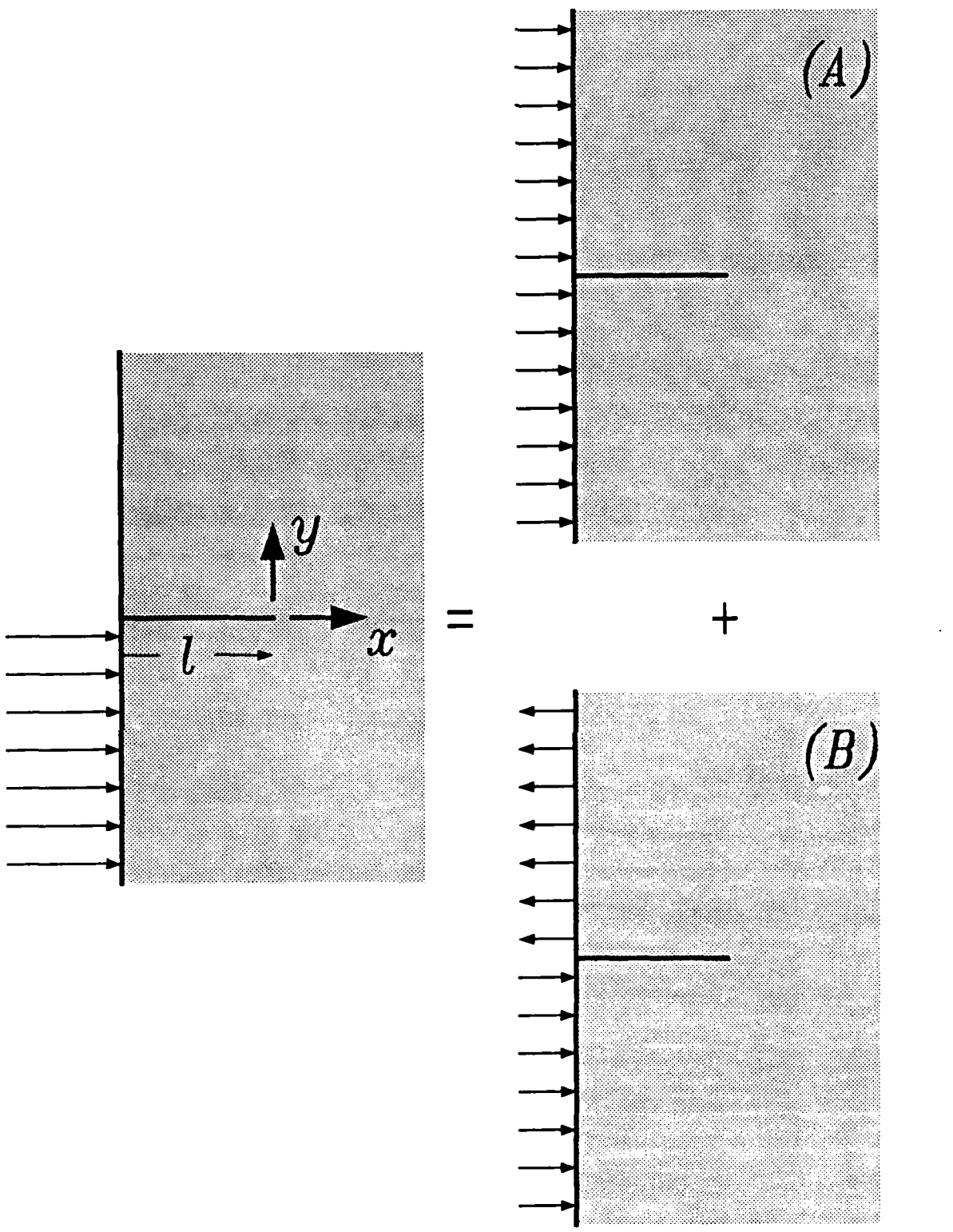

Fig 4

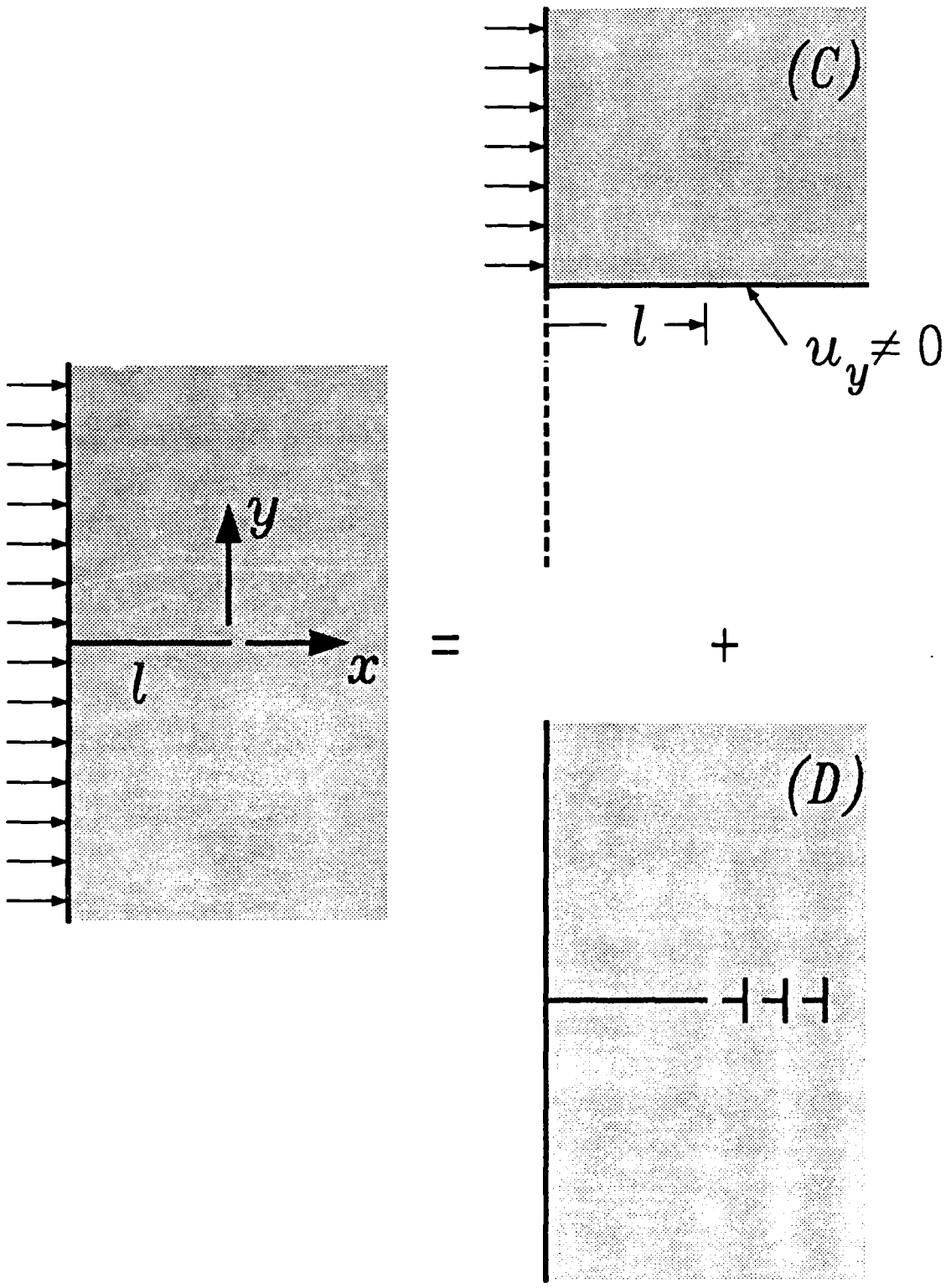

Fig 5

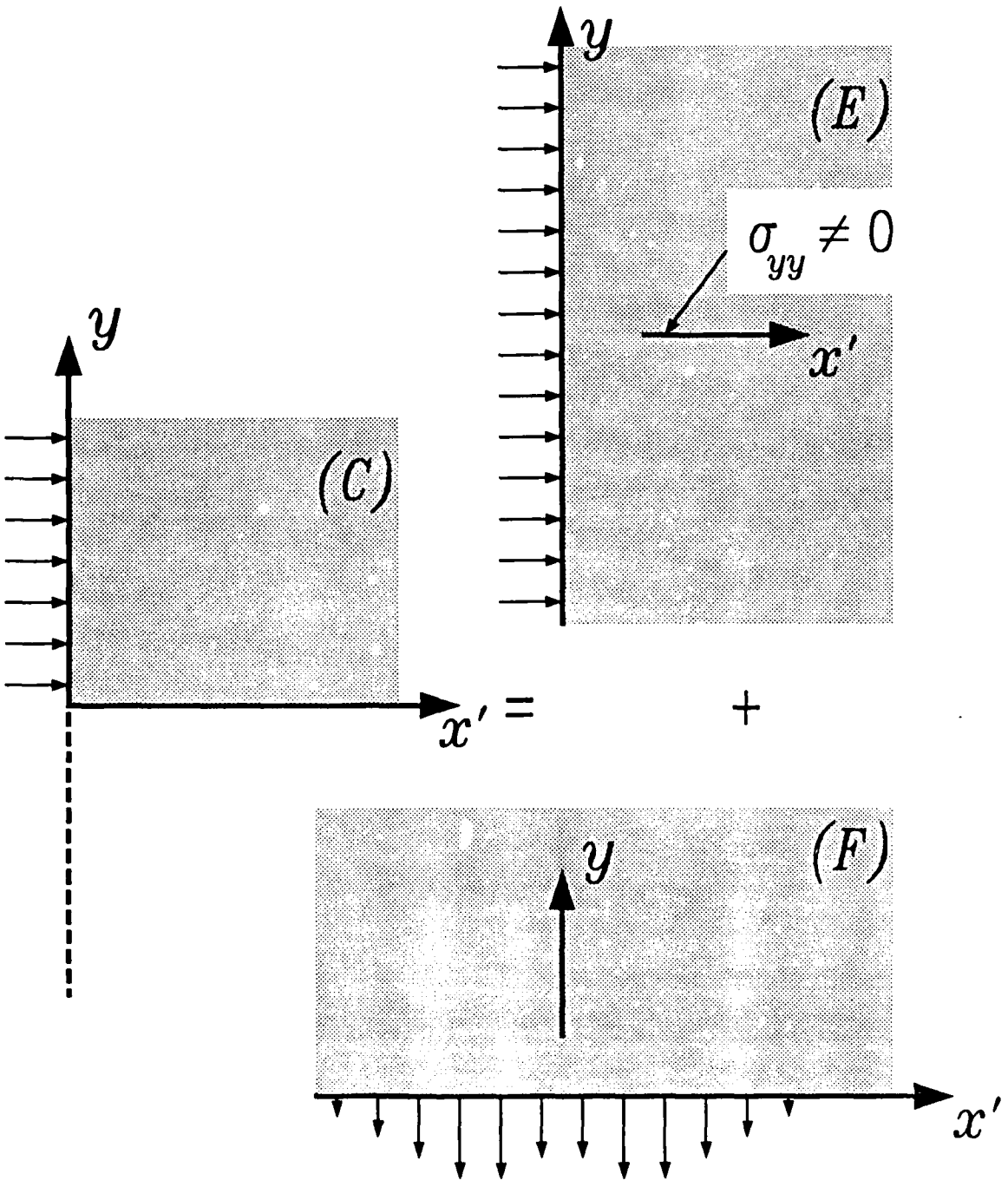

Fig 6

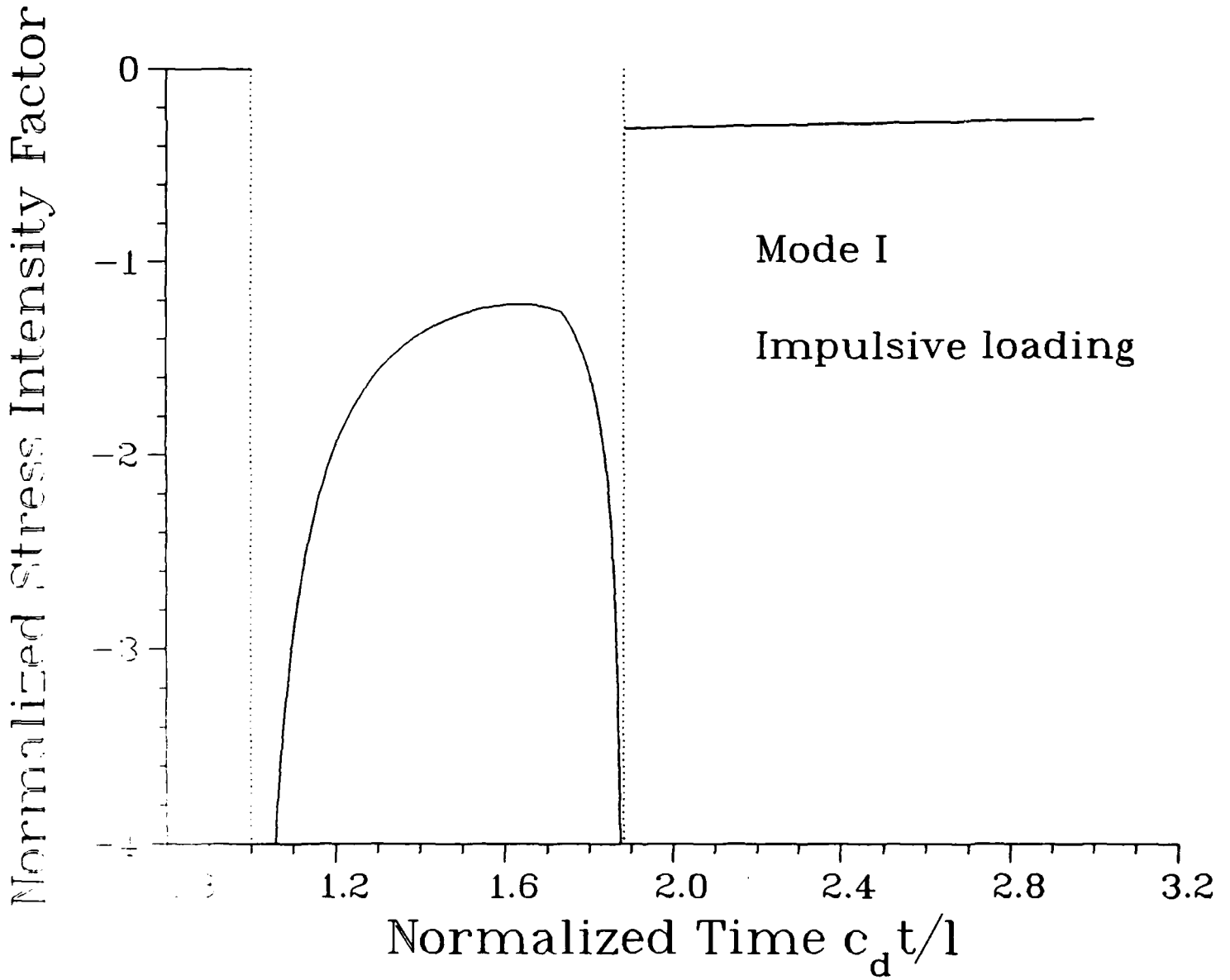
Normalized Stress Intensity Factor
0
-1
-2
-3
-4
1.2
1.6
2.0
2.4
2.8
3.2
Normalized Time $c_d t/l$
Mode I
Impulsive loading

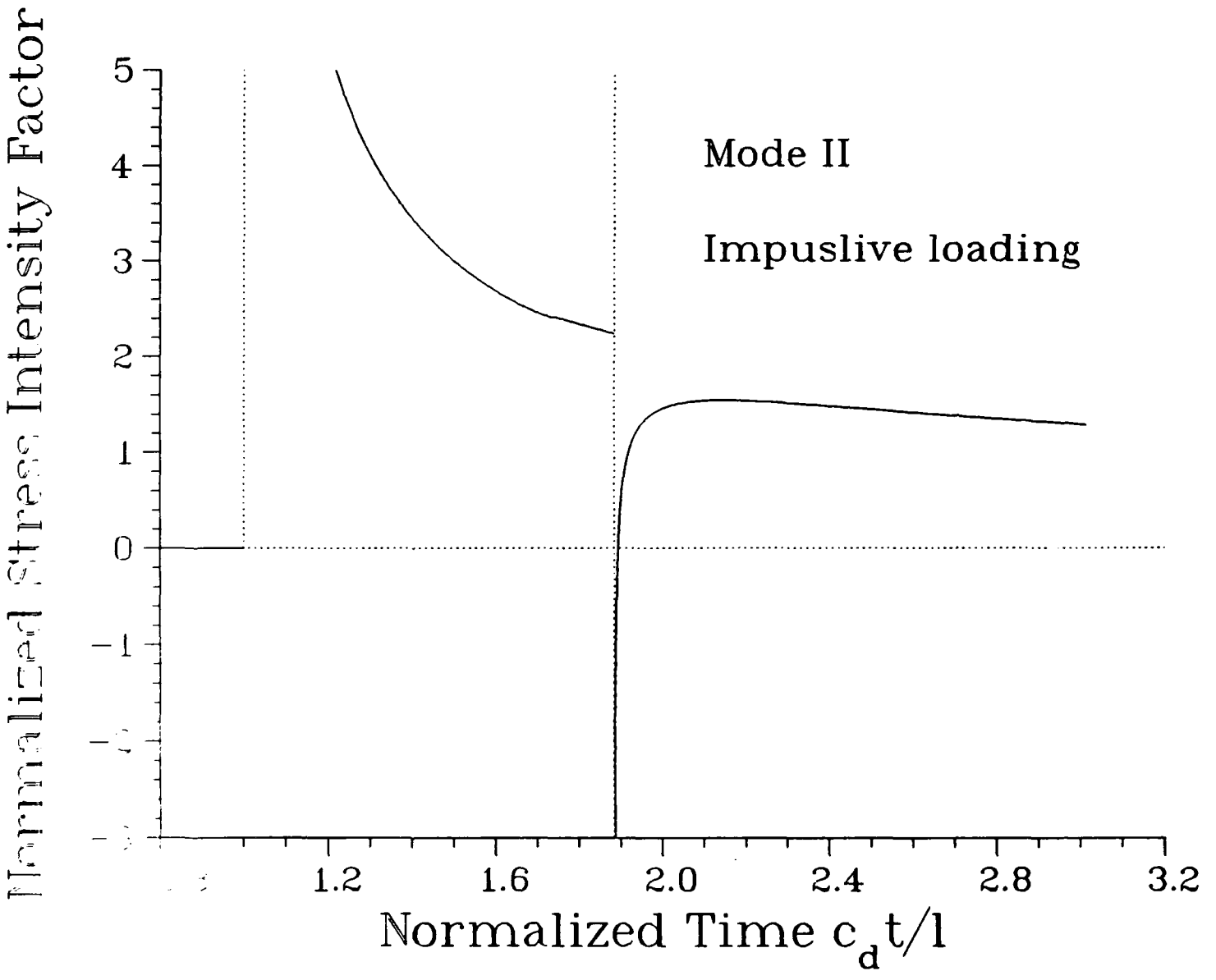
Normalized Stress Intensity Factor
5
4
3
2
1
0
1.2
1.6
2.0
2.4
2.8
3.2
Normalized Time $c_d t/l$
Mode II
Impuslive loading

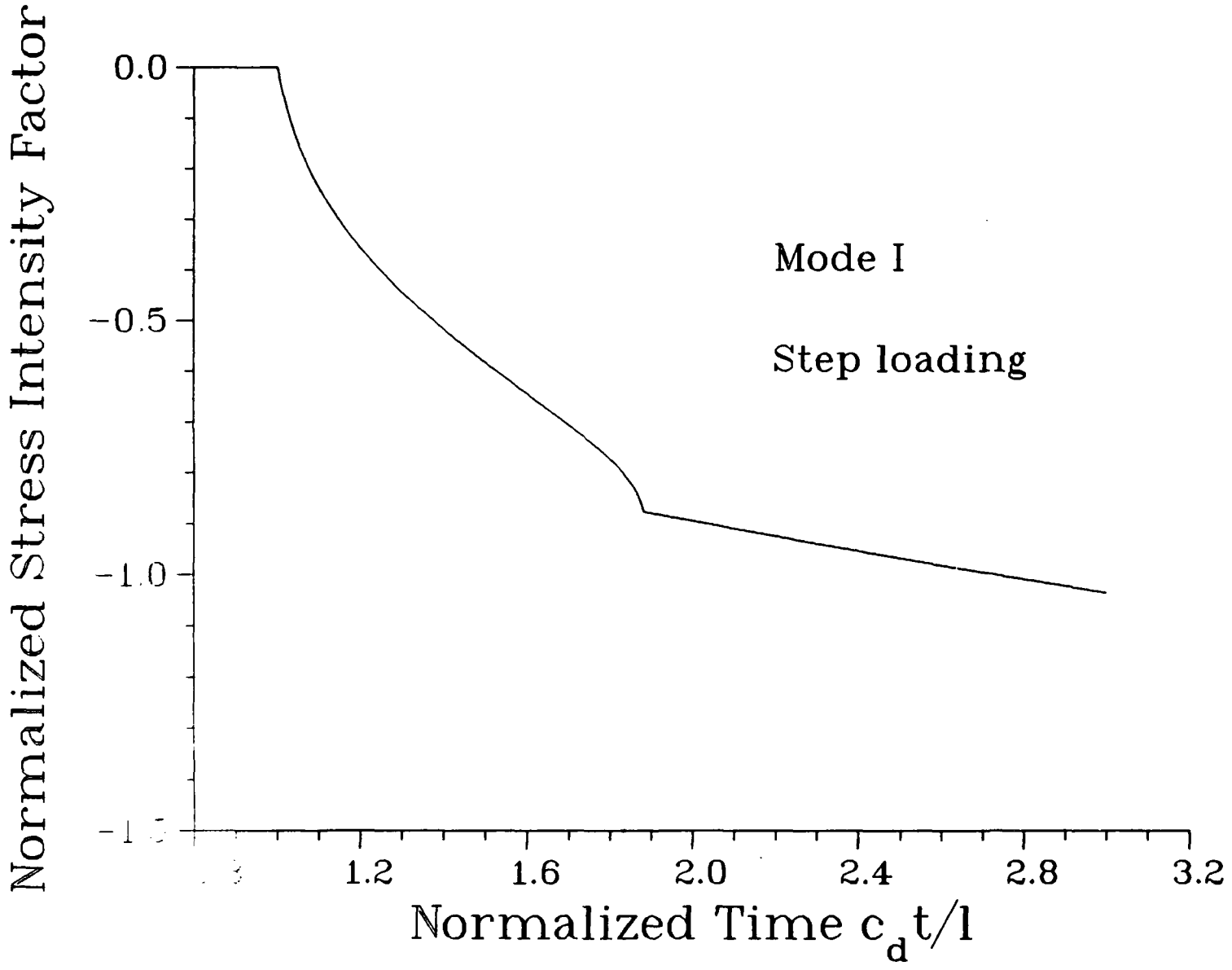
Normalized Stress Intensity Factor
0.0
-0.5
-1.0
1.2
1.6
2.0
2.4
2.8
3.2
Normalized Time $c_d t/l$
Mode I
Step loading

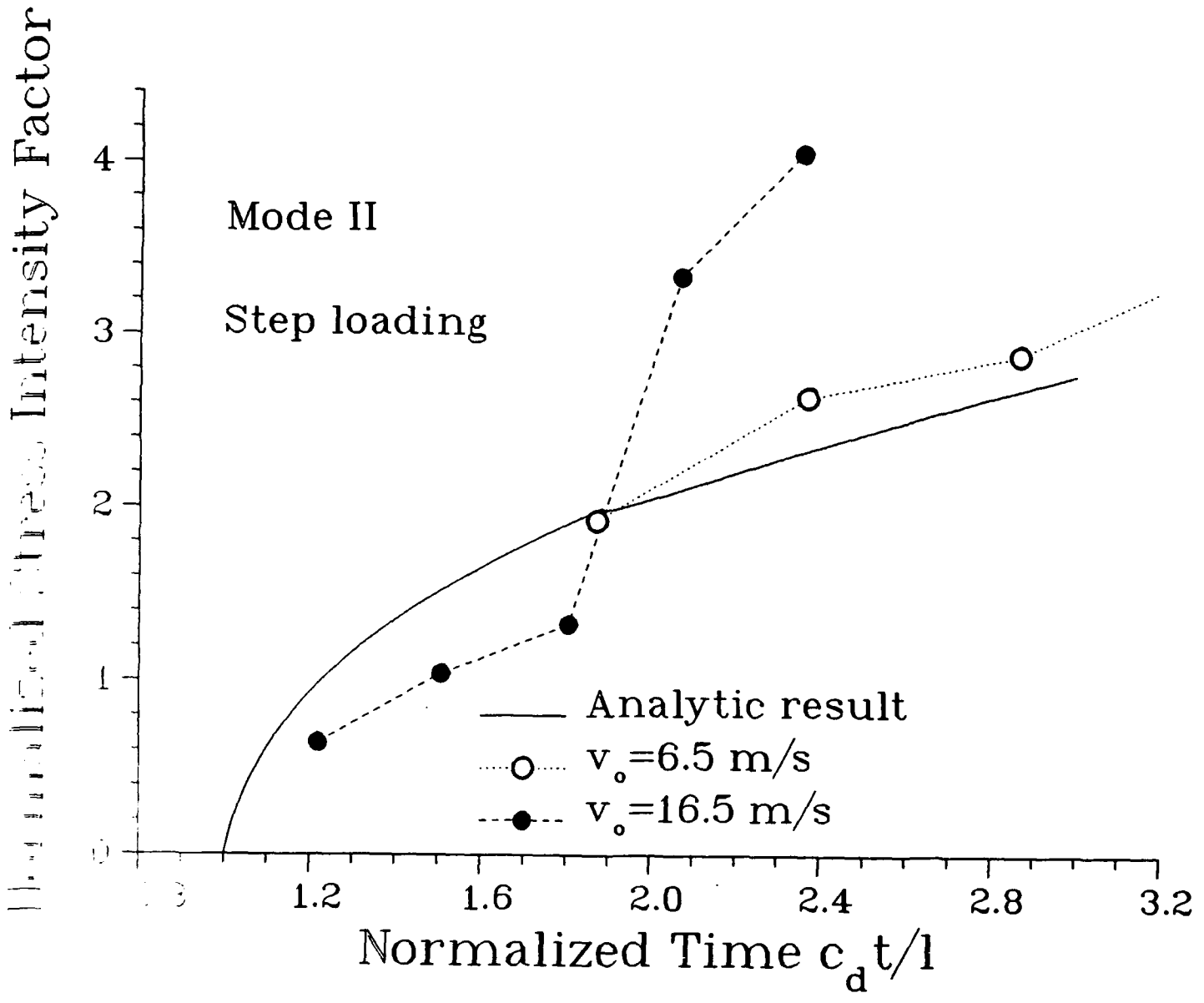
Mode II
Step loading
Analytic result
v_o=6.5 m/s
v_o=16.5 m/s
4
3
2
1
0
1.2
1.6
2.0
2.4
2.8
3.2
Normalized Time $c_d t/l$

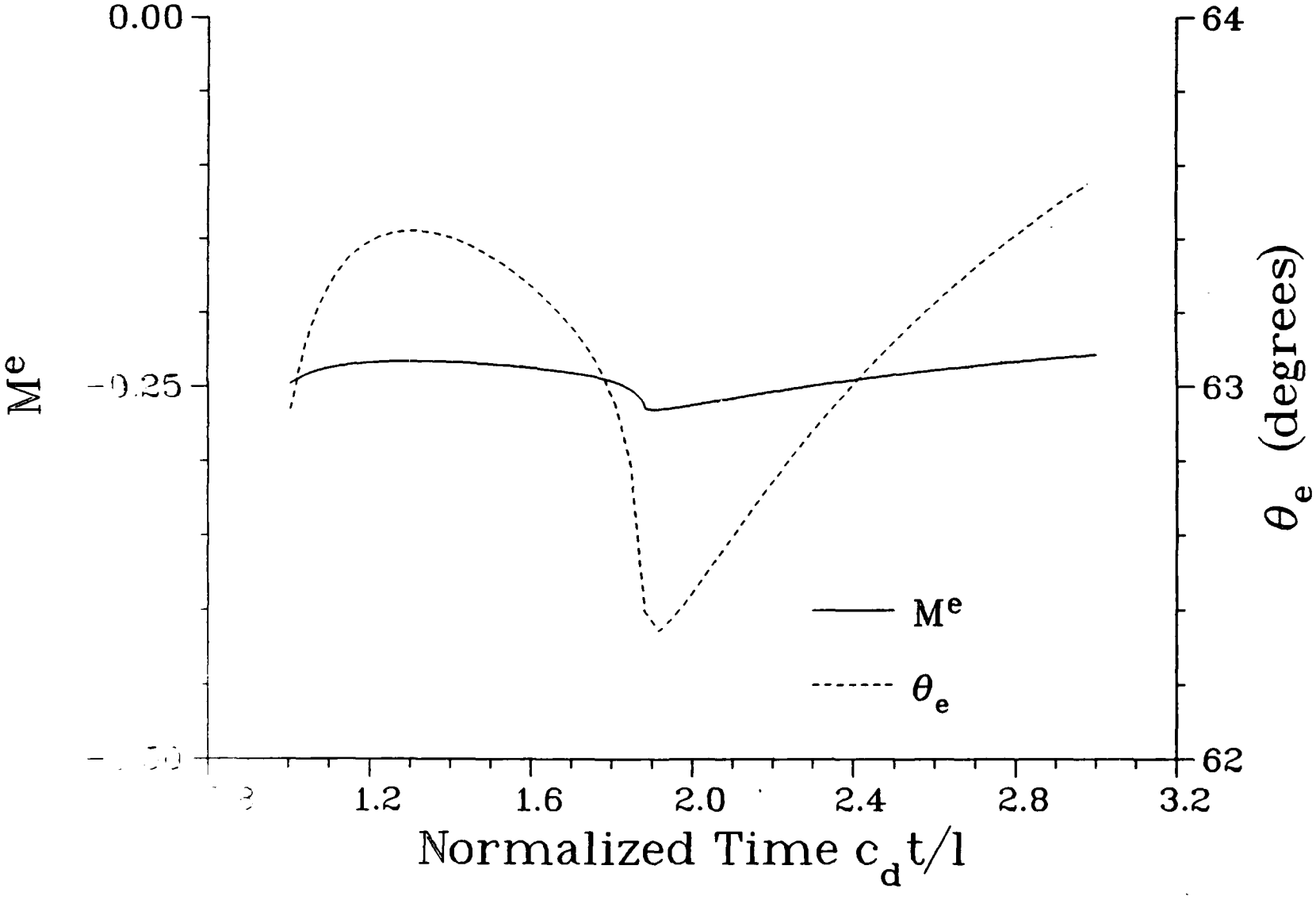
0.00
-0.25
-0.50
M^e
64
63
62
θ_e (degrees)
1.2
1.6
2.0
2.4
2.8
3.2
Normalized Time c_d t/l
M^e
θ_e